Systematic study of the radiative proton capture including the compound, pre-equilibrium, and direct mechanisms

Bing Wang,[1] Yi Xu [2,*] and Stephane Goriely[3]

[1]*Institute of Modern Physics, Chinese Academy of Sciences, Lanzhou 730000, China*

[2]*Extreme Light Infrastructure - Nuclear Physics (ELI-NP), Horia Hulubei National Institute for R&D in Physics and Nuclear Engineering (IFIN-HH), 077125 Buchurest-Magurele, Romania*

[3]*Institut d'Astronomie et d'Astrophysique, Université Libre de Bruxelles, CP-226, 1050 Brussels, Belgium*

A comprehensive study of the proton capture reaction is performed. The three major reaction mechanisms, namely, compound-nucleus capture (CNC), pre-equilibrium capture (PEC), and direct capture (DIC), are simultaneously considered on the basis of the Hauser-Feshbach model, the exciton model, and potential model, respectively. The same nuclear ingredients are consistently used in the three models, and especially the same nucleon-nucleus optical model potential (OMP) ensures that the three components are calculated on the same footing and represents partial fluxes of the same total reaction cross section. For about 2700 nuclei with $8 \leqslant Z \leqslant 100$ lying between the proton drip line and the valley of β stability, the proton capture cross sections and astrophysical reaction rates corresponding to the CNC, PEC, DIC, and total (CNC + PEC + DIC) contributions are computed. The specific nuclear structure ingredients involved in the calculation, namely the nuclear mass, electromagnetic multipole moments, γ-ray strength function, excited-level scheme, spectroscopic factor, and proton-nucleus OMP, are determined from experimental data whenever available and, if not, from global nuclear models. For the reactions involving the targets with mass number $A \geqslant 48$, fair agreements between the calculated proton total capture cross sections and the experimental data are found. For the lightest nuclei ($A < 28$), however, it is found that only the predicted DIC cross sections reproduce the experimental results well, and the total CNC + PEC + DIC contributions tend to overestimate the experimental cross sections. Furthermore, the systematic analysis for the nuclei beyond ^{40}Ca shows that the relative contribution of the proton DIC reaction rate to the total reaction rate increases with increasing temperatures. In particular, the proton DIC reaction rates are comparable to the CNC + PEC reaction rates in the temperature range of the astrophysical p process (2–3 GK) for some open-shell nuclei in the mass region of $70 \leqslant A \leqslant 160$ around the valley of β stability. Such a high DIC contribution stems from the large number of direct transitions to final excited states. In order to better understand the DIC contribution, further experiment and theoretical analyses need to be performed. The impact of the proton DIC reaction rates on the rp- and p-process nucleosynthesis remains to be investigated.

I. INTRODUCTION

Nuclear reactions of astrophysical interest often concern unstable or even exotic species for which no experimental data exist. Although significant efforts have been devoted in the past decades, experimental information only covers a minute fraction of the entire data set required for nuclear astrophysics. Moreover, the energy range for which experimental data is available is restricted to the small range that can be studied by present experimental setups. For all unknown cases, only theoretical predictions can fill the gaps. Specific examples include the p-process nucleosynthesis called for to explain the origin of the 35 stable neutron-deficient p nuclei in the universe [1–13] and the rapid proton-capture process (or rp process) in x-ray bursts [14–18]. They involve a large number of unstable neutron-deficient nuclei for which many different properties have to be determined and cannot be obtained experimentally. One such fundamental property concerns the radiative proton capture reaction which is the main subject of the present study.

The radiative proton capture is generally treated within the statistical Hauser-Feshbach model [19–21]. The model makes the fundamental assumption that the capture process takes place with the intermediary formation of a compound nucleus in thermodynamic equilibrium. The formation of a compound nucleus is usually justified by assuming that the nuclear level density (NLD) in compound nuclei at the projectile incident energy is large enough to ensure an average statistical continuum superposition of available resonances. The energy of the incident particle is then shared uniformly by all the nucleons before releasing the energy by particle emission or γ de-excitation [22]. The compound-nucleus capture (CNC) at the energies of astrophysical interest is known to be the dominant reaction mechanism for medium- and heavy-mass nuclei close to the valley of β stability.

However, when the number of available states in a compound nucleus is relatively small, the capture reaction is

*yi.xu@eli-np.ro

possibly dominated by direct electromagnetic transitions to a bound final state, rather than through the compound-nucleus intermediary. Such direct capture (DIC) proceeds via the excitation of only a few degrees of freedom on a much shorter time scale, reflecting the time taken by the projectile to travel across the target. This mechanism can be satisfactorily described with the perturbative approach known as the potential model [23–26] that has been applied to radiative neutron capture reactions [27–29]. It is now well accepted that the DIC process is important and even dominant at the very low energies of astrophysical interest for light or exotic nuclei systems for which only few or even no resonant states are available [30–34].

The pre-equilibrium capture (PEC), characterized by the high-energy collisions where particles can be emitted after the first direct interaction and before the statistical equilibrium can be reached, lies in between the two extreme CNC and DIC processes. It has been shown [35] that the exciton model can describe the PEC process in a satisfactory way. While for nuclei close to stability the PEC channel dominates above typically 10 MeV, for exotic nuclei with low particle separation energies and a low level density, the PEC process may start to affect the cross section at a few hundred keV because of the difficulty to achieve a full equilibrium for such nuclei [20].

All the CNC, PEC, and DIC mechanisms may contribute to the proton radiative capture reaction, so the total capture cross section is taken as the simple sum of these three contributions. The proton capture on targets in the mass range $20 < A < 63$ has been studied by taking into account the CNC and DIC contributions individually [24,25,36]. In these studies, the CNC through discrete nuclear levels is described by the Breit-Wigner formula where the resonance parameters are obtained from either model predictions or measurements, which is a popular and proper way to treat the light and medium targets with resolved resonances. However, when the number of nuclear levels increases, the NLD is appropriate to deal with the level scheme for CNC in the framework of Hauser-Feshbach model. Moreover, the CNC, PEC, and DIC contributions need to be treated consistently based on the same footing with the same nuclear ingredients especially including the same optical potential and level density.

In the present paper, we perform systematic calculations of the proton capture cross sections and reaction rates for which the CNC, PEC, and DIC contributions are included simultaneously and consistently. We emphasize that (i) the calculations are performed with the updated reaction code TALYS [37–39] in which the models for DIC, CNC, and PEC are incorporated, and (ii) the same set of nuclear structure ingredients are employed to compute all the three contributions. In Sec. II, the potential model for the DIC contribution, the Hauser-Feshbach model for the CNC contribution, and the exciton model for the PEC contribution are described. Detailed nuclear structure ingredients used in these models are provided in Sec. III, including the nuclear ground-state properties, the proton-nucleus interaction potential, the γ-ray strength function, as well as the excitation spectrum deduced from the discrete experimental levels and the NLDs. In Sec. IV, the calculated proton-capture cross sections are compared with available experimental data and extended to the estimate of

the astrophysical reaction rates for about 2700 nuclei with $8 \leqslant Z \leqslant 100$ lying between the proton drip line and the valley of β stability. The summary is given in Sec. V.

II. REACTION MODELS

A. Potential model for direct capture

As a perturbative approach, the potential model is employed to study the proton DIC reaction $A(p, \gamma)B$ describing the transition from the initial scattering state $A + p$ to the final nucleus B with a γ-ray emission. In this model, the incoming proton is scattered directly into the final bound state in nucleus B and the allowed electric-dipole ($E1$), electric-quadrupole ($E2$), and magnetic-dipole ($M1$) transitions to the ground state as well as to all possible excited states in the final nucleus are taken into account. In particular, we consider the transitions to all possible energy levels, including not only the discrete levels but also the continuum described by a combinatorial model of NLD [27–29]. In this way, the proton DIC cross section as a function of incident energy E for $A(p, \gamma)B$ reaction can be expressed as [27]

$$\sigma^{\text{DIC}}(E) = \sum_{x=0}^{E_B^{th}} S_F^x \sigma_{A+p \to B^x + \gamma}^{\text{DIC}}(E) + \int_{E_B^{th}}^{S_p} \langle S_F \rangle$$
$$\times \sum_{I_B^x, \pi_B^x} \rho(E, I_B^x, \pi_B^x) \sigma_{A+p \to B^x + \gamma}^{\text{DIC}}(E) dE_B. \quad (1)$$

In Eq. (1), E is the energy of the incident proton; x corresponds to xth experimentally known energy levels ($x = 0$ means the ground state); E_B^{th} is the excitation energy of the last experimentally known level (smaller than the proton separation energy) in the residual nucleus B. Below E_B^{th}, the sum runs over all available discrete final states. S_F^x is the spectroscopic factor describing the overlap between the antisymmetrized wave function of the initial system $A + p$ and the final state of B^x. Above E_B^{th}, the summation is replaced by a continuous integration over a spin(I_B^x)- and parity(π_B^x)-dependent NLD $\rho(E, I_B^x, \pi_B^x)$ with the cross section and the averaged spectroscopic factor $\langle S_F \rangle$ for all levels.

The potential model calculates the transition matrix element between the initial and the final states by sandwiching the electromagnetic operators in the long-wavelength limit. Taking into account the $E1$, $E2$, and $M1$ transitions, the partial cross section $\sigma_{A+p \to B^x + \gamma}^{\text{DIC}}(E)$ for a transition from the initial $A + p$ system to the final state $B^x + \gamma$ can be written as

$$\sigma_{A+p \to B^x + \gamma}^{\text{DIC}}(E) = \frac{2I_B^x + 1}{Ek(2I_A + 1)(2I_p + 1)}$$
$$\times \sum_{s_f, J_i, l_i, s_i} \left\{ \frac{2}{9} k_\gamma^3 (|M_{E1}|^2 + |M_{M1}|^2) \right.$$
$$\left. + \frac{1}{150} k_\gamma^5 |M_{E2}|^2 \right\}. \quad (2)$$

In Eq. (2), I_B^x, I_A, and I_p are the spin of the nucleus B^x, A, and the proton, respectively, and k_γ is the wave number of the emitted photon. The summations run over the channel spin s_i, orbital angular momentum l_i, and total angular momentum J_i

of the initial system $A + p$, and over the channel spin s_f of the final state. The matrix elements consist of two components, the radial moments ($\mathcal{M}_{E1}$, $\mathcal{M}_{M1}$, $\mathcal{M}_{M2}$) and, if any, the internal moments of the nucleus A [$\mathcal{M}_{M1}^{int}(A)$, $\mathcal{M}_{E2}^{int}(A)$] and proton [$\mathcal{M}_{M1}^{int}(p)$, $\mathcal{M}_{E2}^{int}(p)$], which are given by

$$
\begin{aligned}
M_{E1} &= \mathcal{M}_{E1}, \\
M_{M1} &= \mathcal{M}_{M1} + \mathcal{M}_{M1}^{int}(A) + \mathcal{M}_{M1}^{int}(p), \\
M_{E2} &= \mathcal{M}_{E2} + \mathcal{M}_{E2}^{int}(A) + \mathcal{M}_{E2}^{int}(p).
\end{aligned}
\tag{3}
$$

The complete formula of the matrix elements can be found in Refs. [28,40].

The radial parts (namely the radial wave function ψ) of these matrix elements are obtained by solving the two-body Schrödinger equation

$$
\left[\frac{d^2}{dr^2} - \frac{l(l+1)}{r^2} + \frac{2\mu}{\hbar}\{E - V(E, r)\} \right]\psi = 0
\tag{4}
$$

expressed in the relative coordinate r. Here, $V(E, r)$ is an energy-dependent central potential that consists of the nuclear and Coulomb parts, l is the relative orbital angular momentum, and $\mu = m_A m_p/(m_A + m_p)$ is the reduced mass. For the sake of clarity, ψ is replaced by $\chi_l(E, r)$ for initial scattering system $A + p$ with $E > 0$, and by $\phi_{nl}(r)$ for bound state B^x ($E < 0$) with $E < 0$.

For the scattering system $A + p$, the radial wave functions $\chi_l(k, r)$ (here, $E = \hbar^2 k^2/2\mu$ with the wave number k) behaves asymptotically at large distances as

$$
\chi_l(k, r) \rightarrow e^{i(\delta_l^c + \delta_l)}[\cos(\delta_l)F_l(kr) + \sin(\delta_l)G_l(kr)],
\tag{5}
$$

where δ_l is the phase shift by the nuclear potential, δ_l^c is the Coulomb phase shift, and $F_l(kr)$ and $G_l(kr)$ are the regular and irregular Coulomb wave functions, respectively.

For the bound states B^x, the radial wave functions $\phi_{nl}(r)$ must vanish at infinity and be normalized as

$$
\int_0^\infty |\phi_{nl}(r)|^2 dr = 1,
\tag{6}
$$

where n stands for the radial quantum number.

B. Hauser-Feshbach model for compound-nucleus capture

The Hauser-Feshbach model is built on the fundamental Bohr independence hypothesis that the exit channel loses the memory of the entrance channel by means of the intermediary formation of a compound nucleus reaching a state of thermodynamic equilibrium [19]. Such a formation of a compound nucleus requires its NLD at the excitation energy corresponding to the projectile incident energy to be sufficiently high.

The binary reaction cross section of $A(p, \gamma)B$ by the CNC can be written as

$$
\sigma^{CNC}(E) = \sum_{x=0}^{B} \sigma_{A+p \rightarrow B^x + \gamma}^{CNC}.
\tag{7}
$$

The summation $\sum_{x=0}^{B}$, where the energy-level scheme is represented by the xth excited state ($x = 0$ is the ground state), covers all the ground and all possible excited states of the residual nucleus B. Each state is characterized by a spin I_B^x,

a parity π_B^x, and an excitation energy E_B^x for the residual nucleus B.

Furthermore, the cross section $\sigma_{A+p \rightarrow B^x + \gamma}^{CNC}(E)$ can be expressed as [20,29]

$$
\begin{aligned}
\sigma_{A+p \rightarrow B^x + \gamma}^{CNC}(E) = &\frac{\pi}{k^2} \sum_{J=mod(I_A+I_p,1)}^{l_{max}+I_A+I_p} \sum_{\Pi=-1}^{1} \frac{2J+1}{(2I_A+1)(2I_p+1)} \\
&\times \sum_{J_p=|J-I_A|}^{J+I_A} \sum_{l_i=|J_p-I_p|}^{J_p+I_p} \sum_{\lambda=|J-I_B^x|}^{J+I_B^x} \sum_{l_f=|\lambda-I_\gamma|}^{\lambda+I_\gamma} \delta_{C_p}^\pi \delta_{C_\gamma}^\pi \\
&\times \frac{\langle T_{C_p,l_i,J_p}^J(E)\rangle \langle T_{C_\gamma,l_f,\lambda}^J(E_\gamma)\rangle}{\sum_{Clj} \delta_C^\pi \langle T_{C,l,j}^J(E_C)\rangle} W_{C_p l_i J_p C_\gamma l_f \lambda}^J.
\end{aligned}
\tag{8}
$$

In Eq. (8),

(i) k is the wave number of the relative motion,

(ii) E is the incident energy of the projectile (proton);

(iii) E_γ is the energy of the emitted photon;

(iv) l_{max} is the maximum value of the relative orbital momentum l_i of $A + p$;

(v) l_f is the relative orbital momentum of the residual nucleus B and the photon;

(vi) I_p, J_p, and π_p are the spin, total angular momentum, and parity of the proton, respectively;

(vii) I_γ and π_γ are the spin and parity of the photon, respectively;

(viii) λ is the multipolarity of the photon (total angular momentum of photon) coupled by I_γ and l_f;

(ix) J and Π are the total angular momentum and parity of the compound nucleus, respectively;

(x) C_p is the channel label of the initial system ($p + A$) designated by $C_p = (p, I_p, E, E_A = 0, I_A, \pi_A)$;

(xi) C_γ is the channel label of the final system ($\gamma + B^x$) designated by $C_\gamma = (\gamma, I_\gamma, E_\gamma, E_B^x, I_B^x, \pi_B^x)$;

(xii) $\delta_{C_p}^\pi = 1$ if $\pi_A \pi_p(-1)^{l_i} = \Pi$ and 0 otherwise;

(xiii) $\delta_{C_\gamma}^\pi = 1$ if $\pi_B^x \pi_\gamma(-1)^{l_f} = \Pi$ and 0 otherwise;

(xiv) T is the transmission coefficient;

(xv) $\sum_{Clj} \delta_C^\pi \langle T_{C,l,j}^J(E_C)\rangle$ is the sum of the transmission coefficient for all possible decay channels C; and

(xvi) W is the width fluctuation correction factor for which different approximate expressions are described and discussed in Ref. [41].

Each transmission coefficient T is calculated for all levels with known energy, spin, and parity. If the excitation energy E^x, which is implicit in the definition of the channel C, corresponds to a state in the continuum, an effective transmission coefficient for an excitation-energy bin of width ΔE is defined by the integral

$$
\langle T_{Cjl}^J(E_C)\rangle = \int_{E^x-\Delta E/2}^{E^x+\Delta E/2} \rho(E, J, \Pi) T_{Clj}^J(E_C) dE
\tag{9}
$$

over the NLD $\rho(E, J, \Pi)$. Corresponding to the reaction channels open, the calculation of the transmission coefficient T depends on different nuclear ingredients. For particle emission, T relies on the optical potentials of the two reacting

particles, while T for photon emission is determined by the γ-ray strength function. The detailed nuclear structure ingredients that are used to obtain the transmission coefficients are described in Sec. III.

C. Exciton model for pre-equilibrium capture

For increasing energy or nuclei for which the CNC does not have time to reach thermodynamic equilibrium, PEC or DIC processes may become significant. PEC can occur after the first stage of the reaction but long before statistical equilibrium of the compound nucleus is reached.

One of the most widely used model to describe the PEC mechanism is the (one- or two-component) exciton model [35], in which the nuclear state is characterized at any moment during the reaction by the total energy and the total number of particles (p) above and holes (h) below the Fermi surface. Here, particles and holes are referred to as excitons. Furthermore, it is assumed that all possible ways of sharing the excitation energy between different $p - h$ configurations at the same exciton number $n = p + h$ have *a priori* an equal probability. The basic starting point of the exciton model is a time-dependent master equation, which describes the probability of transitions to more and less complex $p - h$ states as well as transitions to the continuum (emission). Reference [35] provides the complete formalism of the exciton model as included in the TALYS reaction code.

III. NUCLEAR INGREDIENTS

The nuclear inputs required for calculations can be extracted from basic nuclear structure properties. Whenever available, the nuclear ingredients are taken from experiment and, if not, global models are considered. The nuclear ingredients involved in the present study are described below.

A. Nuclear mass, electromagnetic multipole moment, and photon strength function

Nuclear masses are taken from the 2020 Atomic Mass Evaluation [42] whenever available. When not available, theoretical masses are predicted by the Hartree-Fock-Bogoliubov (HFB) method based on the effective nucleon-nucleon interaction of Skyrme type, namely the HFB-21 mass model [43].

The nuclear magnetic-dipole (μ_1) and electric-quadrupole (Q_2) moments appearing in the potential model calculation are taken from the experimental data compilation of [44]. When no data are available, the single-particle model is used for predicting the nuclear magnetic-dipole moment, while the nuclear deformation parameter (β_2) obtained within the HFB-21 mass model [43,45] are adopted to estimate the electric-quadrupole moments.

Large-scale derivations of the γ-ray strength function have been conducted with the use of the HFB plus quasiparticle random phase approximation (QRPA) models [46–49]. The HFB + QRPA model is known to be an accurate tool to estimate the γ-ray strength function in both closed- and open-shell nuclei. In the present calculation, the γ-ray strength functions obtained from the Gogny HFB + QRPA model based on the D1M interaction [48] are used in the Hauser-Feshbach model to compute the electromagnetic dipole transmission coefficients. The contribution of an $M1$ zero-energy limit (also known as "upbend") is taken into account in the calculation of the de-excitation strength, as detailed in Ref. [48].

B. Nuclear level scheme and spectroscopic factor

Nuclear level scheme is a crucial ingredient for the potential model calculation, as shown by Eqs. (1) and (9). For the DIC calculations, it is well accepted that the predicted cross sections are in qualitatively good agreement with experimental results as long as all the details of the excitation spectrum are known experimentally [50,51]. For this reason, whenever available, the discrete experimental level schemes are taken from RIPL-3 library [52]. Note that the main contribution to the DIC cross section often results from transitions to the ground state or to a small number of low-lying states, provided the selection rules allow for the considered electromagnetic transitions [28].

Nevertheless, for most nuclei, only few experimental levels, if any, are available. In this situation, we must resort to a theoretical level spectrum determined from a NLD model. The microscopic HFB plus a combinatorial approach [53] has proven its capacity to estimate the nonstatistical spin and parity dependence of the NLD and to reproduce the low-lying cumulative number of levels. Based on this model, the spin- and parity-dependent NLDs as well as the partial ph densities are deduced, which are consistently used in the present calculations of the CNC, PEC, and DIC contributions.

Determining the spectroscopic factor (S_F) remains a difficult problem. Usually, light nuclei, closed-shell nuclei, and nuclei at low excitation energy have discrete levels with a high-purity single-particle configuration. However, away from the magic numbers, or at increasing excitation energy, residual interactions and couplings of the single-particle motion to other degrees of freedom, distribute the spectroscopic strength of a single-particle state among several nuclear levels.

In the present study, for the discrete level contributions in Eq. (1), the spectroscopic factors reported in Refs. [36,54,55] are taken into account and, if not available, $S_F = 0.347$ is used. Note that this spectroscopic factor for proton capture are identically taken from the corresponding values for the neutron capture, as considered in Ref. [29]. Here, given that $A + p \rightarrow B$ and $C + n \rightarrow D$ are the mirror pair (A and B have the inverted proton and neutron number in regard to C and D), it can be assumed that the proton S_F of $A + p \rightarrow B$ is identical to the neutron S_F of $C + n \rightarrow D$ [57,58]. Meanwhile, it must be acknowledged that appropriate shell-model calculations [24,36,56] may help in providing the proton spectroscopic factors for specific nuclear levels, as well as some systematics. In the present study, the energy-dependent spectroscopic factor $\langle S_F \rangle(E) = 0.1 + 0.33 \exp(-0.8E)$ derived in Ref. [56] for neutron captures is considered and used in the integral contribution of Eq. (1).
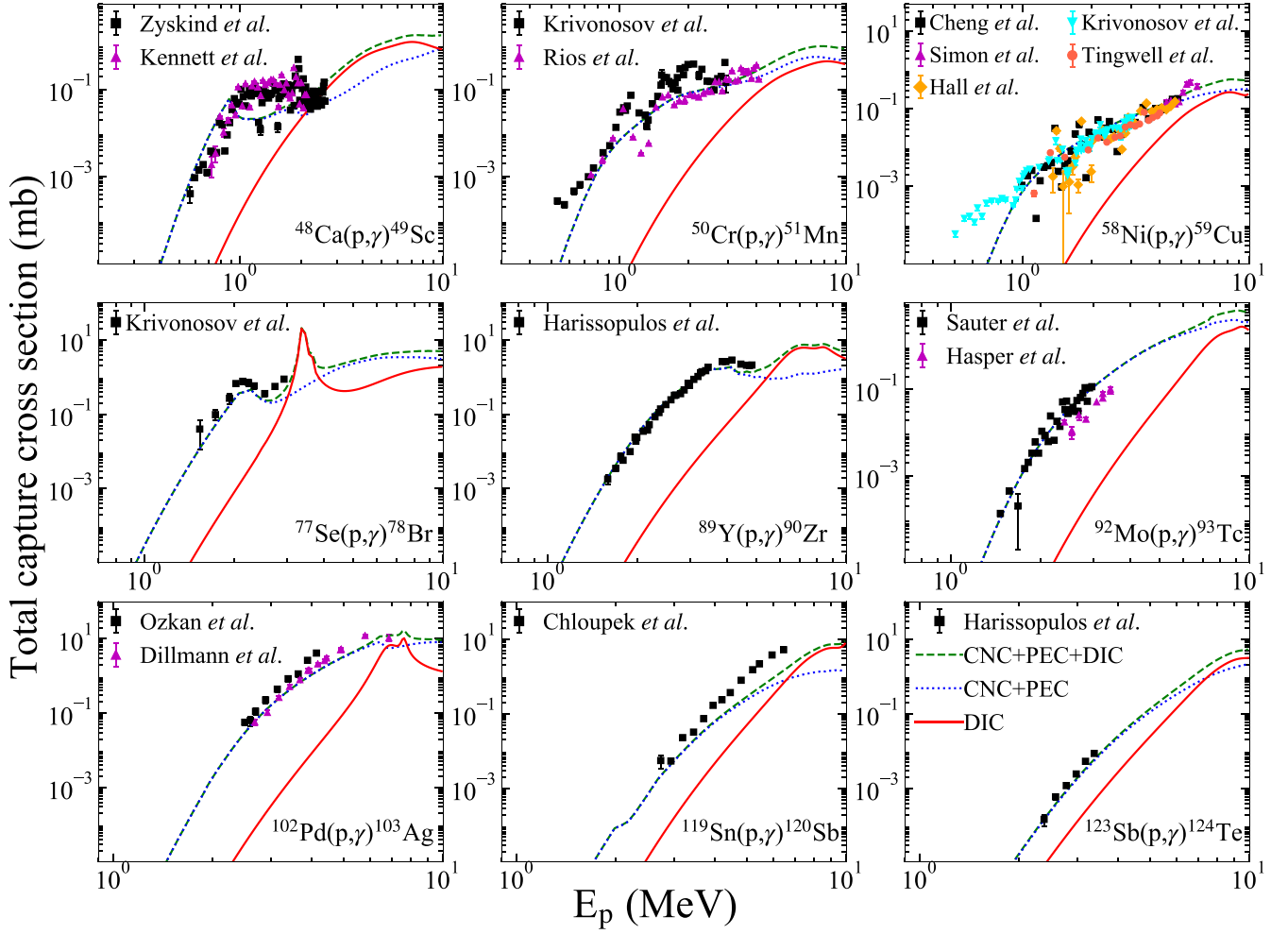
FIG. 1. Comparison of the calculated and experimental proton capture cross sections as a function of the proton energy E_p for nine nuclei. The green dashed lines, the blue dotted lines, and the red solid lines correspond to the total (CNC + PEC + DIC), the CNC + PEC, and the DIC contributions, respectively. The experimental data are taken from Refs. [67,68] for ^{48}Ca$(p,\gamma)^{49}$Sc, [69,70] for ^{50}Cr$(p,\gamma)^{51}$Mn, [69,71–74] for ^{58}Ni$(p,\gamma)^{59}$Cu, [69] for ^{77}Se$(p,\gamma)^{78}$Br, [75] for ^{89}Y$(p,\gamma)^{90}$Zr, [76,77] for ^{92}Mo$(p,\gamma)^{93}$Tc, [78,79] for ^{102}Pd$(p,\gamma)^{103}$Ag, [80] for ^{119}Sn$(p,\gamma)^{120}$Sb, and [75] for ^{123}Sb$(p,\gamma)^{124}$Te.

C. Nuclear potential

The optical model potential (OMP) is another essential input for the calculations of the proton capture reactions. In principle, both the phenomenological and microscopic folding OMPs could be employed to systematically study the (p,γ) cross sections and the reaction rates.

The global phenomenological Woods-Saxon (WS) OMP for the system of (nucleon + target) is described in detail in Ref. [59], which has been extensively tested on experimental data of nucleon-induced reactions with incident energies from 1 keV up to 200 MeV and target masses ranging from $A = 24$ to $A = 209$. This OMP is based on a smooth and unique functional form for the energy dependence of the potential depths and the physically constrained geometry parameters. The explicit expression reads

$$U(E, r) = -V_v(E, r) - iW_v(E, r) - iW_s(E, r)$$
$$+ V_{s.o.}(E, r) + V_c(r), \qquad (10)$$

where V_v and $W_{v,s}$ are the real and imaginary components of the volume-central (v) and surface-central (s) potentials, respectively, $V_{s.o.}$ the spin-orbit potential, and V_c the Coulomb potential. The central potentials are separated into energy-dependent well depths and energy-independent form factor, namely,

$$V, W_v(E, r) = V, W_v(E) \times f(r, R_v, a_v) \qquad (11)$$

and

$$W_s(E, r) = -4a_s W_s(E) \times d(f(r, R_s, a_s))/dr. \qquad (12)$$

The form factor f is given by the Woods-Saxon shape

$$f(r, R_i, a_i) = (1 + \exp[(r - R_i)/a_i])^{-1}, \qquad (13)$$

where the geometry parameters are the radius $R_i = r_i A^{1/3}$ with A being the atomic mass number and the diffuseness a_i. The parametrization of the proton OMP as a function of Z, A, and incident energy E used in the present calculations can be found in Ref. [59].

In parallel, the Bruyères-le-Châtel renormalization [60] of the Jeukenne-Lejeune-Mahaux potential [61], referred to as JLMB, is a global semimicroscopic nucleon-nucleus OMP adjusted on experimental data of $A = 30$–240 nuclei and for the energies ranging from 10 keV up to 200 MeV [62,63]. The JLMB potential has been phenomenologically renormalized in Refs. [60,64] to improve the agreement between experimental and predicted observables for a large set of data.

The previous study [65,66] indicates that for most (p, γ) and (γ, p) reactions involving nuclei lying between the proton drip line and the valley of β stability, the ratios of the reaction rates computed by the WS OMP to those computed by the JLMB OMP are within a factor of 2. The JLMB OMP has been systematically studied in capture reactions for nuclear astrophysics applications [21,29]. For these reasons, only the phenomenological WS OMP is adopted in the present study.

IV. RESULTS

TALYS [39] is a software for the simulation of nuclear reactions. It provides a complete description of all reaction channels and observables to estimate the total reaction probability as well as the competition between the various open channels, by taking into account all types of direct, pre-equilibrium, and compound mechanisms. The nuclear models to cover these three main reaction mechanisms, as presented in Sec. II, have been included in TALYS. For the nuclear ingredients in TALYS, the experimental information is considered whenever available, and if not, various theoretical results derived from local and global nuclear-structure models are included, as described in Sec. III.

In addition to our original implementation of neutron DIC in the TALYS code [29], we have updated the latest v1.96 TALYS version [39] by including new functionalities for proton DIC calculations, which up to now has never been extensively tested and studied. It is now possible to compute all the CNC, PEC, and DIC contributions for proton capture reactions, consistently and simultaneously, making use of the same input physics. Based on this updated TALYS version, systematic calculations of the cross sections and the astrophysical reaction rates $N_a \langle \sigma v \rangle$ (where N_a is the Avogadro number, and v is the relative velocity between target and projectile) for proton capture including the CNC, PEC, and DIC contributions are performed for about 2700 nuclei with $8 \leqslant Z \leqslant 100$ lying between the proton drip line and the valley of β stability. The corresponding results are discussed below.

A. Comparison with experiments

To verify the proton capture reaction model, in Fig. 1 the calculated total proton capture cross sections including the CNC, PEC, and DIC mechanisms (green dashed lines) are compared with the experimental data for nine proton capture reactions on medium and heavy nuclei, namely, ^{48}Ca, ^{50}Cr, ^{58}Ni, ^{77}Se, ^{89}Y, ^{92}Mo, ^{102}Pd, ^{108}Cd, and ^{123}Sb. It can be seen that the experimental cross sections are fairly well reproduced by the total (DIC + PEC + CNC) capture results, as shown in Fig. 1. This confirms that the model is capable of predicting the proton capture cross section. The CNC + PEC (blue dotted
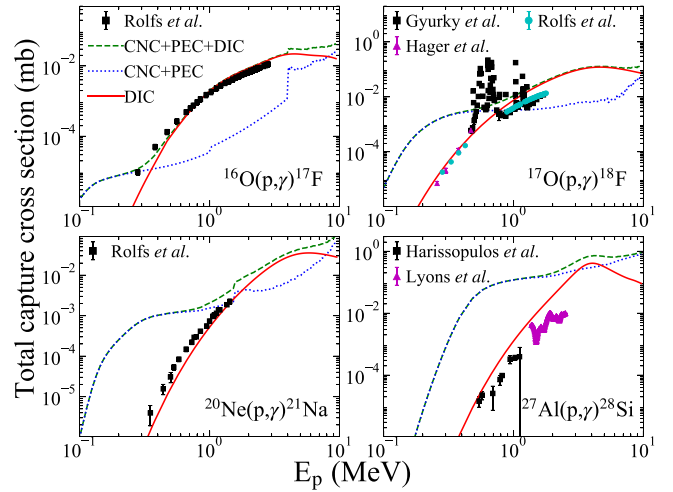

FIG. 2. Comparison of the calculated proton capture cross sections and the experimental data for four light nuclei. The green dashed lines, the blue dotted lines, and the red solid lines correspond to the total (CNC + PEC + DIC), the CNC + PEC, and the DIC contributions, respectively. The experimental data are taken from Ref. [23] for ^{16}O$(p, \gamma)^{17}$F, [23,81,82] for ^{17}O$(p, \gamma)^{18}$F, [83] for ^{20}Ne$(p, \gamma)^{21}$Na, and [84,85] for ^{27}Al$(p, \gamma)^{28}$Si.

lines) and the DIC (red solid lines) cross sections are individually plotted in Fig. 1.

Similarly in Fig. 2, the calculated proton capture cross sections corresponding to the total (DIC + PEC + CNC), the CNC + PEC, and the DIC mechanisms are compared with the available experimental data for four proton capture reactions on very light targets ^{16}O, ^{17}O, ^{20}Ne, and ^{27}Al. It can be found that the total CNC + PEC + DIC contributions, or more specifically the CNC contribution, tend to overestimate the cross sections, especially at the lower reaction energies. For the CNC reaction mechanism described by the Hauser-Feshbach model, it is always assumed that the number of nuclear levels available to the incident nucleon in the compound nucleus is large enough and that their energy and width are randomly distributed within the contributing energy interval to ensure a continuum superposition of resonances. However, these conditions might not be fulfilled when none or only a small number of resonances are available experimentally, especially for light nuclei with $A < 28$; in this case, the Hauser-Feshbach model for the CNC contribution is expected to overestimate the cross section.

For these four specific reactions shown in Fig. 2, the numbers of experimentally known resonances in the interval of $[S_p, S_p + 1]$ MeV (S_p is the proton separation energy) for the compound nuclei ^{17}F, ^{18}F, ^{21}Na, and ^{28}Si are 0, 9, 2, and 20, respectively, which are quite lower than the average number of energy levels extracted from level density in an interval of 1 MeV. On the other hand, the DIC contribution is seen in Fig. 2 to reproduce fairly well the experimental cross sections. Special attention should therefore be paid when extrapolating the statistical predictions to light nuclei. A more suited approach would be to combine the potential model for DIC
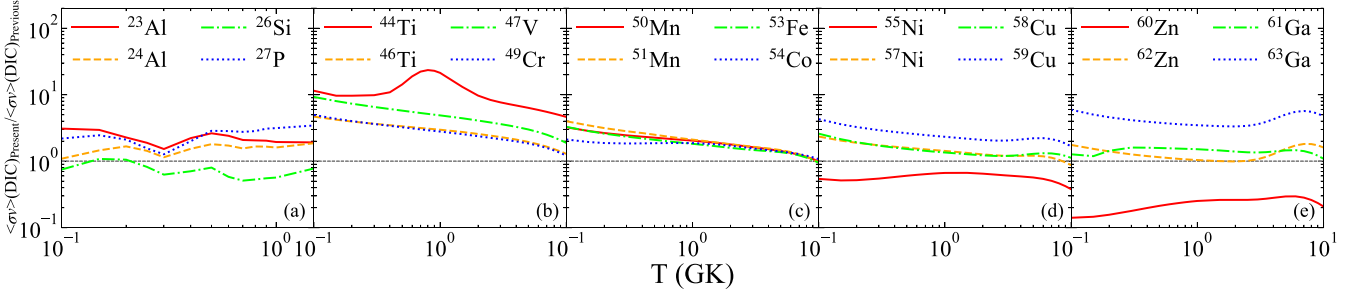
FIG. 3. Ratios of the present proton DIC reaction rates to those results taken from previous studies as a function of the temperature T for the target nuclei with $A = 23$–27 [36] and $A = 44$–63 [24].

B. Comparison with previous studies

The proton DIC reaction rates are compared in Fig. 3 with previous studies for four nuclei with mass number $A = 23$–27 [36] and 16 nuclei with $A = 44$–63 [24]. Such studies used detailed shell-model calculations to determine the level spectra, proton spectroscopic factors, and electromagnetic transition probabilities. Doing so, their predictions of nuclear structure properties are expected to be more reliable for the calculation of the DIC than those obtained in the present approach. They are, however, restricted to light $A \leqslant 63$ nuclei. It can be seen in Fig. 3 that our predictions remain within a factor of 5 with respect to the shell-model-based rates for most nuclei, though the nuclear ingredients may be rather different. A higher proton DIC reaction rate is obtained by the present study (except for ^{55}Ni and ^{60}Zn) and mainly stems from the transitions not only to the discrete experimental levels but also to the additional high-lying levels deduced from the nuclear level densities.

Our total (DIC + PEC + CNC) proton capture reaction rates are compared with the REACLIB results [86,87] in Fig. 4 for the $N = 50$ isotonic chain. For most nuclei, especially the stable species, the ratios are found to be close to one, which demonstrates a fair agreement between both results. Note that the largest discrepancies between the present and REACLIB calculations are found for the two nuclei with the largest and lowest proton numbers, namely ^{84}Se $(Z = 34)$ and ^{99}In $(Z = 49)$, reflected by ratios approaching a factor of 8 in Fig. 4. Since REACLIB rates only include the CNC contribution and make use of different nuclear ingredients including nuclear mass, level scheme, photon strength function, and nuclear potential, such discrepancies are not surprising. In particular, different level schemes and optical potentials may have significant impact on the reaction rate calculations. In REACLIB, the shifted Fermi-gas NLD is considered to build the level scheme, while the experimental levels plus the levels extracted from the microscopic HFB plus combinatorial approach are used in the present study. For the nuclear potential, the JLM potential is taken into account in REACLIB, while the global potential of Koning-Delaroche [59] is considered in the present study.

C. Systematic analysis of the contributions to proton capture mechanism

Figure 1 showed that the present proton DIC + PEC + CNC model is suitable for nuclei with $A > 48$, while for $A < 28$, the applicability of the present model is unclear, as illustrated in Fig. 2. Considering such a comparison and the adequacy of the nuclear level density to meet the requirement of the model calculations, we restrict ourselves here to nuclei heavier than ^{40}Ca, i.e., about 2700 nuclei with $20 \leqslant Z \leqslant 100$ lying between the proton drip line and the valley of β stability.

The calculated proton capture reaction rate corresponding to the DIC, CNC + PEC, and total (CNC + PEC + DIC) contributions are compared in Fig. 5 for eight isotonic chains of $N = 20$, 28, 35, 43, 50, 62, 77, and 82 at a temperature $T = 3$ GK ($T_9 = 3$). It can be seen that the total reaction rate generally decreases along with the increasing number of protons. Such a phenomenon is partially related to the number of the energy levels in two energy intervals, (i) the range $[S_p, S_p + E_p]$ in which the compound nucleus forms via CNC (here, E_p is on the order of 1 MeV and S_p is the proton separation energy), and (ii) the range $[0, S_p]$ in which the residual nucleus is generated via the DIC transitions and the CNC decays. For the nuclei on an isotonic chain, S_p usually decreases with the increasing number of proton, and thus the nuclei in the exotic proton-rich region, especially close to the proton drip line, have the smallest S_p and correspondingly the smallest number of available states in both energy intervals. Consequently, the energy levels in both energy intervals involved in proton DIC and CNC (and allowed by selection rules), become scarce, leading to a decrease of the corresponding (p, γ) cross sections and reaction rates. This description can be demonstrated by comparing the proton capture reaction rates (Fig. 5) for the isotonic chains of $N = 50$ with the numbers of experimental levels in $[0, S_p]$ and $[S_p, S_p + 1$ MeV$]$ as well as the nuclear level density just above the highest known experimental level (see Fig. 6). All these quantities follow a similar pattern.

In Fig. 5, it is also interesting to see that for some open-shell nuclei around the valley of β stability, the proton DIC reaction rate is comparable to the CNC + PEC rate or even dominates the total capture mechanism for a few species. For these nuclei, the DIC contribution leads to an increase of the total proton capture reaction rate by at most one order of magnitude at $T = 3$ GK. In order to better understand
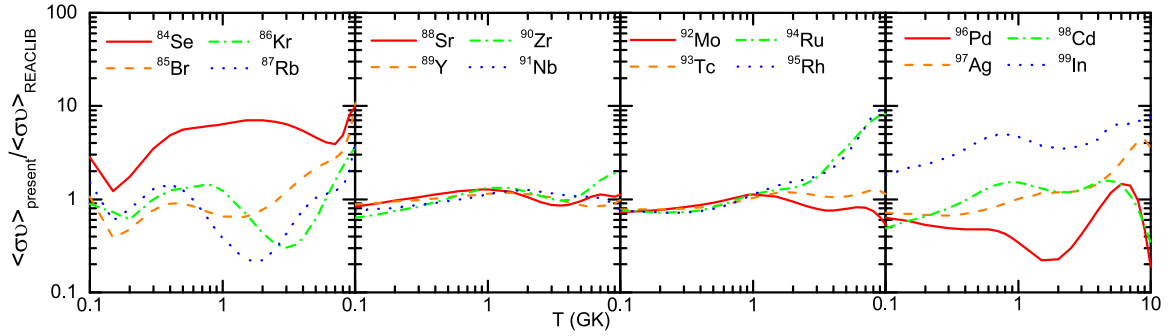
FIG. 4. Ratios of the present proton total (DIC + CNC + PEC) reaction rates to the REACLIB results [86,87] as a function of the temperature T for the target nuclei with $N = 50$.

this behavior, the relative contributions to the DIC reaction rates from the transitions to the discrete experimental levels and to the levels extracted from nuclear level density in the continuum energy range are investigated in Fig. 7. In addition, to study the impact of the continuum energy range [the integral contribution in Eq. (1)], two different choices for the spectroscopic factor are considered, namely, the default energy-dependent spectroscopic factor $\langle S_F \rangle (E) = 0.1 + 0.33 \exp(-0.8E)$ (see Sec. III B) and the constant spectroscopic factor $\langle S_F \rangle = 0.347$, as adopted for the discrete level contribution [56]. For $N = 50$ and $N = 77$ isotones, Fig. 7 (upper panel) illustrates, for both parametrizations of the spectroscopic factor, the relative contributions to the DIC reaction rates stemming from transitions to the discrete experimental levels and to the levels extracted from nuclear level density in the continuum energy range. From Figs. 5 ($N = 50$ and $N = 77$) and 7 (upper panel), it is clear that, for low-Z isotones, the main contribution to the DIC reaction rate originates dominantly from the transitions to the levels extracted from the nuclear level density in the continuum energy range. The exponentially decreasing value of the adopted

spectroscopic factor for increasing excitation energies (see Sec. III B) is compensated by the exponential increase of the number of levels, leading still to a significant contribution of the DIC.

Figure 7 (upper panels) also illustrates that the relative contributions to the DIC reaction rates from the transitions to these two kinds of levels are not so sensitive to the choice of spectroscopic factor, so that the assumptions made on the spectroscopic factor does not drastically change the conclusion concerning the possible significant contribution of the DIC. The DIC reaction rates calculated with both parametrizations of the spectroscopic factor for the levels in the continuum energy range are further compared in Fig. 7 (lower panels), in which the ratios of both calculations are plotted for $N = 50$ and $N = 77$ isotones. It can be seen that for most nuclei, the discrepancy is smaller than 60%. This result is in agreement with the relatively similar behavior found for the relative contributions to the DIC reaction rate shown in Fig. 7 (upper panels).

As shown in Fig. 5, we also find that the relative DIC contribution to the total reaction rate increases with decreasing
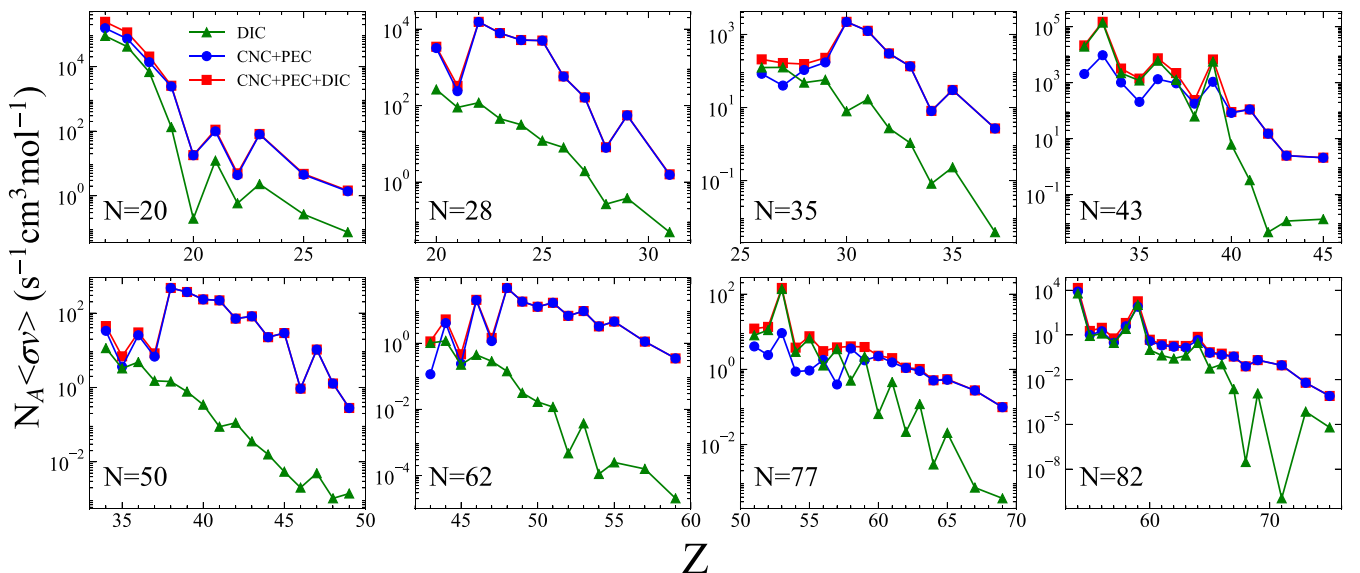

FIG. 5. Proton DIC, CNC + PEC, and total (CNC + PEC + DIC) reaction rates for the nuclei of eight isotonic chains with $N = 20$, 28, 35, 43, 50, 62, 77, and 82 at $T = 3$ GK.
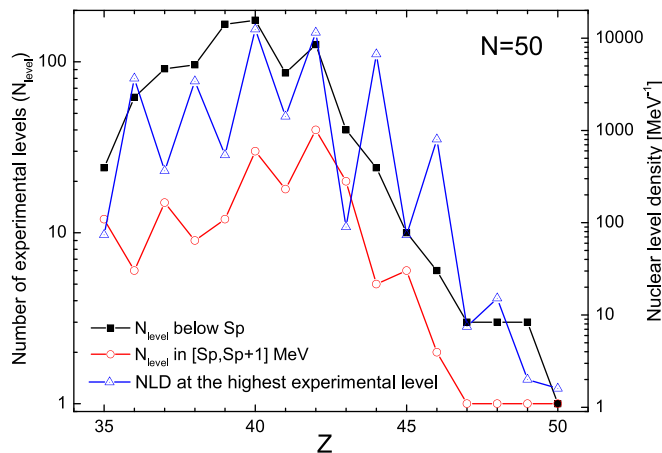
FIG. 6. Numbers of experimental energy levels in the intervals $[0,S_p]$ and $[S_p, S_p+1$ MeV$]$ (S_p is the proton separation energy) and the nuclear level density just above the highest known experimental level for nuclei along the $N = 50$ isotone.

Z along an isotone, or equivalently with increasing $(N - Z)$. For example, along the $N = 50$ isotone, ^{85}Br has a quite larger relative DIC contribution than ^{98}Cd. A similar result was found for neutron captures on the neutron-rich side. In

particular, within the same model, Fig. 3 of Ref. [29] shows that, for Sn and Pb isotopes, the DIC relative contribution increases with increasing N, or equivalently with increasing $(N - Z)$. Such a behavior indicates that, for both proton and neutron captures, the relative DIC contribution is related to the difference $(N - Z)$. This can be further explained by the present DIC potential model that is built on a single-particle scheme. More specifically, a large hole configuration available to nucleons, reflected by a large $(N - Z)$ difference, leads to a large capture probability [the square of the modulus of the wave function computed in Eq. (4)], since transitions to already occupied states in the final nucleus are forbidden within the potential model. In particular, $Z = N$ nuclei are characterized by a relatively low DIC contribution, as illustrated in Fig. 5.

The relative contribution of DIC, represented by the ratio of DIC reaction rate to the total (CNC + PEC + DIC) reaction rate, is shown in Fig. 8 as a function of the temperature for 32 nuclei in the mass region of $50 \leqslant A \leqslant 120$. Note that the results are presented in terms of four isotonic chains ($N = 28$, 40, 50, and 64). It can be seen that the impact of the DIC contribution to the total reaction rate depends on the temperature. At increasing temperature, the relative contribution of DIC becomes considerable, especially for some open shell nuclei with $N = 40$ and 64. Compared to closed shell nuclei,
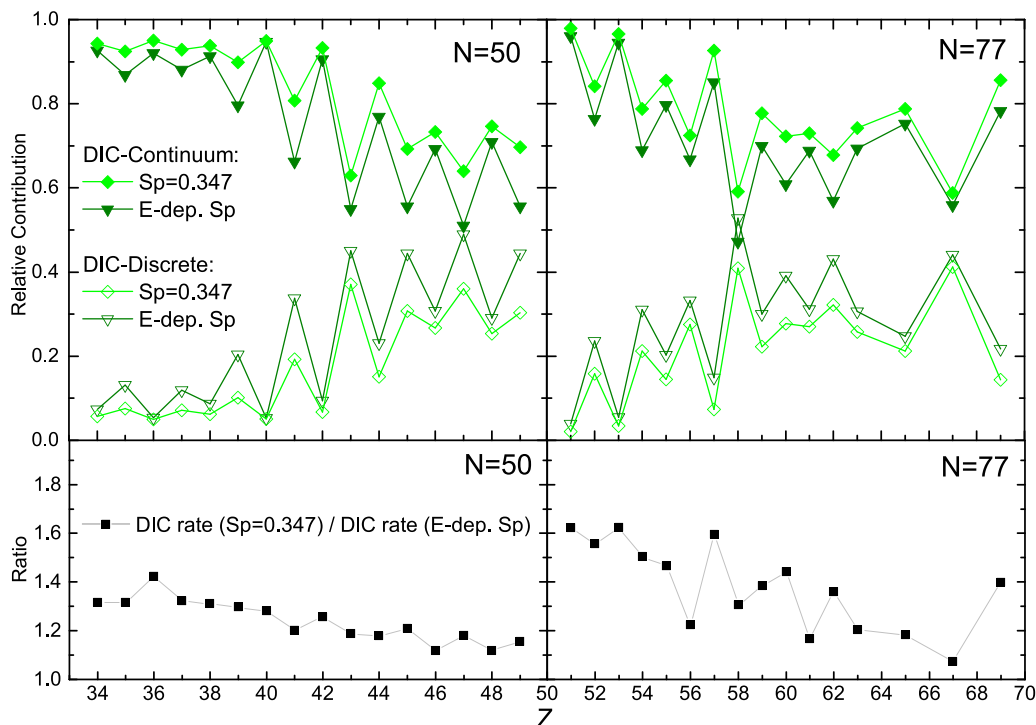

FIG. 7. (Upper panel) Contributions to the DIC reaction rates from the transitions to the discrete experimental levels [the summation part of Eq. (1)] relative to one coming from the levels extracted from the nuclear level density in the continuum energy range [the integral part of Eq. (1)]. Two calculations are shown, one using the energy-dependent spectroscopic factor $\langle S_F \rangle(E) = 0.1 + 0.33 \exp(-0.8E)$ and another one with a constant spectroscopic factor $\langle S_F \rangle = 0.347$. Calculations correspond to nuclei along the $N = 50$ (left panels) and $N = 77$ (right panels) isotones. (Lower panel) Ratios of the DIC reaction rates calculated with the constant spectroscopic factor $\langle S_F \rangle = 0.347$ used for the levels extracted from nuclear level density in the continuum energy range [the integral part of Eq. (1)] to those with the energy-dependent spectroscopic factor $\langle S_F \rangle(E) = 0.1 + 0.33 \exp(-0.8E)$ for nuclei along $N = 50$ and $N = 77$ isotones.
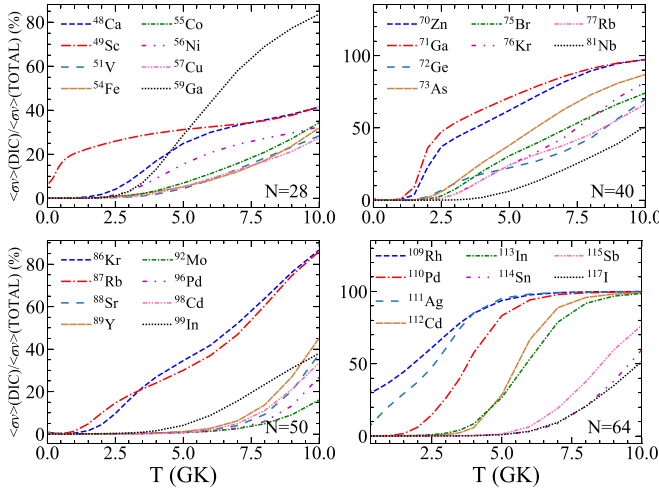
FIG. 8. Relative contributions of the proton DIC reaction rates to the total (CNC + PEC + DIC) reaction rates for nuclei from four isotonic chains with $N = 28, 40, 50$, and 64 as a function of the temperature.

open shell nuclei have a larger probability for multiparticle emissions, due to their lower threshold energies against multiparticle emissions. Therefore, when the temperature increases (namely, the reaction energy increases), the relative contribution of the CNC + PEC reaction rate to the total (CNC + PEC + DIC) reaction rate for open shell nuclei tend to decrease even more due to the opening of additional emission channels, leading to a relative increase of the DIC contribution.

Figure 9 represents in the (N, Z) plane the ratio between the total (CNC + PEC + DIC) reaction rates and the (CNC + PEC) reaction rates (without DIC contribution) for the nuclei beyond ^{40}Ca at the temperatures of $T = 1, 2, 3$, and 4 GK, respectively. It can be seen that as the temperature increases from 1 to 4 GK, the ratio becomes larger, thus the relative contribution of the DIC to the total proton capture reaction rate increases. Figure 9 also shows that the DIC mechanism hardly contributes to the total proton capture rate for the exotic nuclei approaching the proton drip line, while for the species close to the valley of β stability, the DIC contribution gradually becomes significant. Furthermore, the DIC contribution to the total capture reaction rate is enhanced for the open shell nuclei in the mass region of $70 \leqslant A \leqslant 160$.

As an example, as shown in Fig. 10, the DIC cross section of ^{148}Nd(p, γ) ^{149}Pm exceeds the CNC + PEC contribution at $E_p \lesssim 3.5$ MeV (E_p is the energy of the incident proton), which leads to a significant DIC contribution to the reaction rate at $T \simeq 2.5$ GK. Note that in Fig. 10, the DIC cross section with transition to the ground state merely accounts for a small proportion of the entire DIC contribution. Such a high DIC cross section stems from the large number of transitions to final excited states and is consequently sensitive to the nuclear spectrum included in the potential model. A future measurement of such a reaction cross section in this mass region could shed light on such a possible DIC contribution. Note that the proton DIC is currently studied in the temperature range of 1–4 GK, which covers the typical temperature range of relevance for the astrophysical rp and p processes. The impact of the DIC contribution to the proton
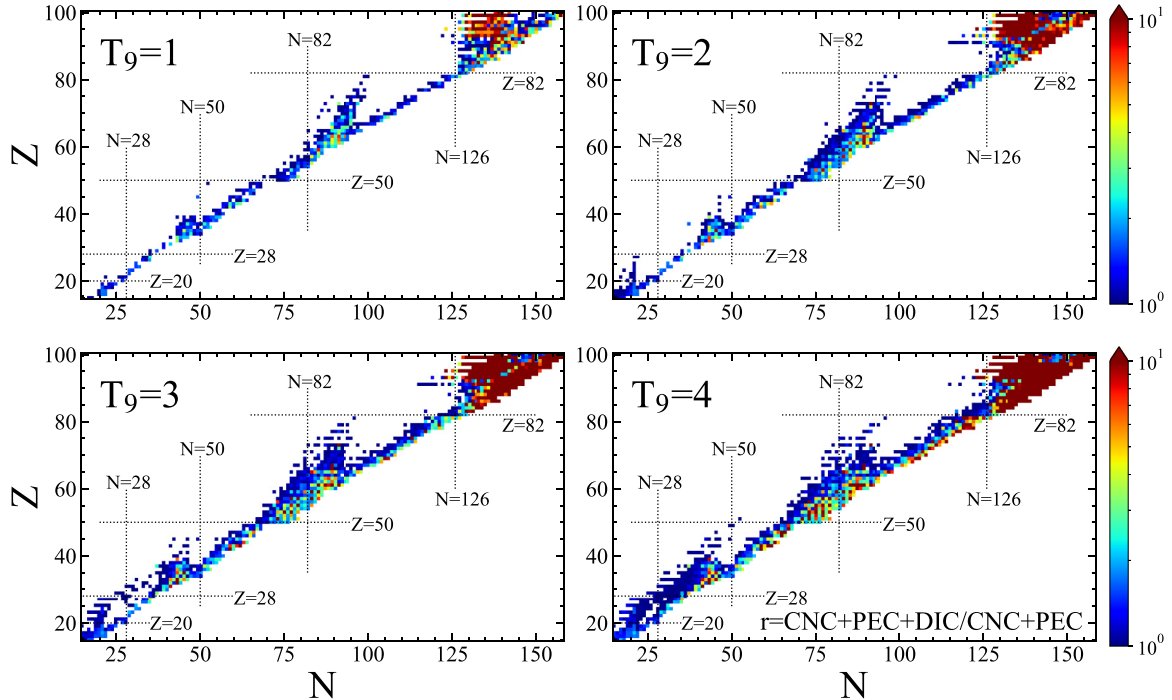

FIG. 9. Representations in the (N, Z) plane of the ratio r between the total (CNC + PEC + DIC) reaction rates and the (CNC + PEC) reaction rates at the temperatures of $T = 1, 2, 3$, and 4 GK, respectively, for about 2700 nuclei with $20 \leqslant Z \leqslant 100$ lying between the proton drip line and the valley of β stability. Only nuclei for which the $r > 1$ are shown.
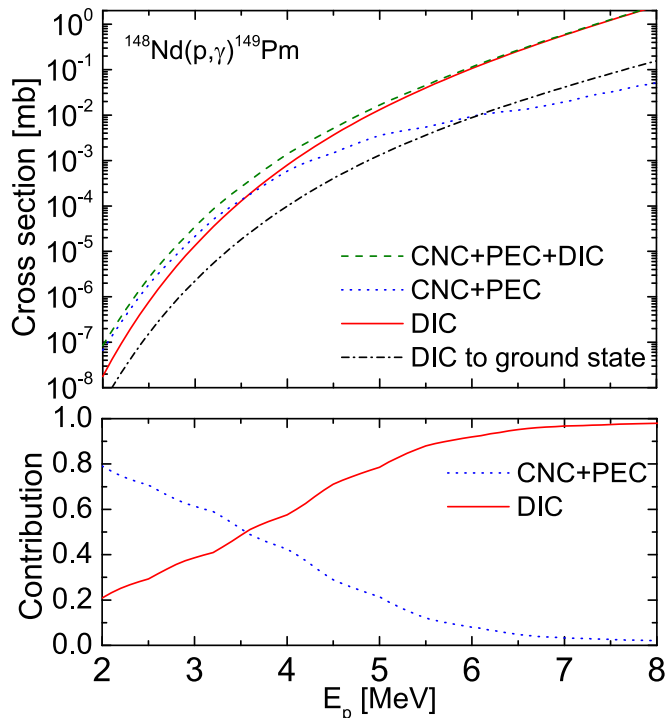
FIG. 10. Upper panel: Calculated cross section of ^{148}Nd(p, γ) ^{149}Pm. The green dashed, blue dotted line, and red solid lines correspond to the total (CNC + PEC + DIC), CNC + PEC, and the DIC contributions, respectively. The black dash-dot line shows the DIC cross section to the ground state only. Lower panel: Relative contribution of the DIC and the CNC + PEC cross sections of ^{148}Nd(p, γ) ^{149}Pm. E_p is the energy of the incident proton.

capture reaction rates on the rp- and p-process nucleosynthesis remains to be investigated.

V. SUMMARY

In this paper, the proton capture reactions have been studied comprehensively by taking into account the three CNC, PEC, and DIC reaction mechanisms simultaneously in the framework of the modern reaction code TALYS. A special emphasis has been put on the description of DIC mechanism on the basis of the potential model, in which the electric dipole ($E1$), the electric quadrupole ($E2$), and magnetic dipole ($M1$) transitions are all included. Of particular relevance, the same nuclear inputs are consistently used to determine the three contributions, and the same nucleon-nucleus optical potential ensures that the three components are calculated on the same footing and represents partial fluxes of the same total reaction cross section. The nuclear structure ingredients involved in the present study, namely the nuclear mass, electromagnetic multipole moments, γ-ray strength function, excited level scheme, spectroscopic factor, and proton-nucleus interaction potential are taken from experimental data whenever available and, if not, from global nuclear models.

The proton capture cross sections and astrophysical reaction rates corresponding to the CNC, PEC, DIC, and total

(CNC+PEC+DIC) contributions have been systematically computed for about 2700 nuclei with $8 \leqslant Z \leqslant 100$ lying between the proton drip line and the valley of β stability. It is shown that the calculated proton total capture cross sections including all the three mechanisms are in fair agreement with experimental data for the targets with mass number $A \geqslant 48$. For the light nuclei with $A < 28$, however, the CNC calculation tends to overestimate the experimental cross sections, especially at the lower reaction energies. For such light species, none or only a small number of resonances exist, while the Hauser-Feshbach model describing the CNC mechanism assumes a resonance capture is still possible. On the other hand, the DIC model is found to describe fairly well the experimental cross sections. It is further expected that for light nuclei involving a few resolved resonant states, a combination of the DIC reaction model and the Breit-Wigner calculation of the resonance capture should provide a better description of the cross section. Some discrepancies are found between the present calculations and results from previous studies; these mainly stem from the different nuclear ingredients used in the calculations, especially the level schemes.

Furthermore, a systematic analysis for nuclei beyond ^{40}Ca is performed. When considering different isotonic chains covering $N = 20$ to 82, the total reaction rate generally decreases with increasing proton number. For the proton-rich nuclei approaching the proton drip line, their proton separation energy S_p decreases and correspondingly the numbers of energy levels. Therefore, the allowed DIC transitions and CNC decays involving these levels are scarce, and the generated (p, γ) cross section decreases.

It is found that the relative contribution of the proton DIC reaction rate to the proton total capture reaction rate generally increases for increasing temperatures. At $T = 3$ GK, for some open-shell nuclei in the mass region of $70 \leqslant A \leqslant 160$ around the valley of β stability, the proton DIC reaction rate becomes comparable to the CNC+PEC rates, hence increases the rate by at most one order of magnitude. Such a high DIC contribution stems from the large number of direct transitions to final excited states and is consequently sensitive to the nuclear spectrum included in the potential model. Future measurements of the cross section in this mass region could shed light on the possible DIC contribution. Moreover, a detailed sensitivity analysis, especially with respect to the adopted NLD, spectroscopic factor and optical model potential, still needs to be performed within the present framework, and is postponed to a future work. Meanwhile, the impact of the proton DIC reaction rate on the rp and p processes remains to be investigated.

---

[1] M. Arnould and C. Brihaye, Astron. Astrophys. **1**, 193 (1969).

[2] S. E. Woosley and W. M. Howard, Astrophys. J. Suppl. Series **36**, 285 (1978).

[3] M. Rayet, N. Prantzos, and M. Arnould, Astron. Astrophys. **227**, 271 (1990).

[4] M. Arnould and S. Goriely, Phys. Rep. **384**, 1 (2003).

[5] S. Fujimoto, M. Hashimoto, O. Koike, K. Arai, and R. Matsuba, Astrophys. J. **585**, 418 (2003).

[6] W. Rapp, J. Gorres, M. Wiescher, H. Schatz, and F. Käppeler, Astrophys. J. **653**, 474 (2006).

[7] T. Hayakawa, N. Iwamoto, T. Kajino, T. Shizuma, H. Umeda, and K. Nomoto, Astrophys. J. **685**, 1089 (2008).

[8] C. Travaglio, R. Gallino, T. Rauscher, N. Dauphas, F. K. R. Roepke, and W. Hillebrandt, Astrophys. J. **795**, 141 (2014).

[9] M. Pignatari, K. Gobel, R. Reifarth, and C. Travaglio, Int. J. Mod. Phys. E **25**, 1630003 (2016).

[10] T. Rauscher, N. Nishimura, R. Hirschi, G. Cescutti, A. S. J. Murphy, and A. Heger, Mon. Not. R. Astron. Soc. **463**, 4153 (2016).

[11] N. Nishimura, T. Rauscher, R. Hirschi, A. S. J. Murphy, G. Cescutti, and C. Travaglio, Mon. Not. R. Astron. Soc. **474**, 3133 (2018).

[12] C. Travaglio, T. Rauscher, A. Heger, M. Pignatari, and C. West, Astrophys. J. **854**, 18 (2018).

[13] A. Choplin, S. Goriely, R. Hirschi, N. Tominaga, and G. Meynet, Astron. Astrophys. **661**, A86 (2022).

[14] R. K. Wallace and S. E. Woosley, Astrophys. J. Suppl. Series **45**, 389 (1981).

[15] H. Schatz, A. Aprahamian, J. Gorres, M. Wiescher, T. Rauscher, J. F. Rembges, F.-K. Thielemann, B. Pfeiffer, P. Möller, K.-L. Kratz, H. Herndl, B. A. Brown, and H. Rebel, Phys. Rep. **294**, 167 (1998).

[16] S. Wanajo, Astrophys. J. **647**, 1323 (2006).

[17] J. José, F. Moreno, A. Parikh, and C. Iliadis, Astrophys. J. Suppl. Series **189**, 204 (2010).

[18] A. Parikh, J. José, G. Sala, and C. Iliadis, Prog. Part. Nucl. Phys. **69**, 225 (2013).

[19] W. Hauser and H. Feshbach, Phys. Rev. **87**, 366 (1952).

[20] S. Goriely, S. Hilaire, and A. J. Koning, Astron. Astrophys. **487**, 767 (2008).

[21] E. Vagena, M. Axiotis, and P. Dimitriou, Phys. Rev. C **103**, 045806 (2021).

[22] G. R. Satchler, *Introduction to Nuclear Reactions* (Macmillan Press Ltd., London, 1980).

[23] C. Rolfs, Nucl. Phys. A **217**, 29 (1973).

[24] J. L. Fisker, V. Barnard, J. Görres, K. Langanke, G. Martínez-Pinedo, and M. Wiescher, At. Data Nucl. Data Tables **79**, 241 (2001).

[25] C. Iliadis, J. M. D'Auria, S. Starrfield, W. J. Thompson, and M. Wiescher, Astrophys. J. Suppl. Ser. **134**, 151 (2001).

[26] P. Descouvemont, J. Phys. G **35**, 014006 (2008).

[27] S. Goriely, Astron. Astrophys. **325**, 414 (1997).

[28] Y. Xu and S. Goriely, Phys. Rev. C **86**, 045801 (2012).

[29] Y. Xu, S. Goriely, A. J. Koning, and S. Hilaire, Phys. Rev. C **90**, 024604 (2014).

[30] H. Oberhummer and G. Staudt, in *Nuclei in the Cosmos*, edited by H. Oberhummer (Springer Verlag, Heidelberg, 1991), p. 29.

[31] H. Beer, C. Coceva, P. V. Sedyshev, Y. P. Popov, H. Herndl, R. Hofinger, P. Mohr, and H. Oberhummer, Phys. Rev. C **54**, 2014 (1996).

[32] S. Chiba, H. Koura, T. Hayakawa, T. Maruyama, T. Kawano, and T. Kajino, Phys. Rev. C **77**, 015809 (2008).

[33] J. T. Huang, C. A. Berutulani, and V. Guimaraes, At. Data Nucl. Data Tables **96**, 824 (2010).

[34] Y. Xu, K. Takahashi, S. Goriely, M. Arnould, M. Ohta, and H. Utsunomiya, Nucl. Phys. A **918**, 61 (2013).

[35] A. J. Koning and M. C. Duijvestijn, Nucl. Phys. A **744**, 15 (2004).

[36] H. Herndl, J. Görres, M. Wiescher, B. A. Brown, and L. Van Wormer, Phys. Rev. C **52**, 1078 (1995).

[37] A. J. Koning, S. Hilaire, and M. Duijvestijn, in *Nuclear Data for Science and Technology*, edited by O. Bersillon *et al.* (EDP Sciences, Paris, 2008), p. 211.

[38] A. J. Koning and D. Rochman, Nucl. Data Sheets **113**, 2841 (2012).

[39] A. Koning, S. Hilaire, and S. Goriely, Eur. Phys. J. A **59**, 131 (2023); see also https://tendl.web.psi.ch/tendl_2021/talys.html.

[40] P. Descouvemont, *Theoretical Models for Nuclear Astrophysics* (Nova Science, New York, 2003).

[41] S. Hilaire, C. Lagrange, and A. J. Koning, Ann. Phys. **306**, 209 (2003).

[42] W. J. Huang, M. Wang, F. G. Kondev, G. Audi, and S. Naimi, Chin. Phys. C **45**, 030002 (2021).

[43] S. Goriely, N. Chamel, and J. M. Pearson, Phys. Rev. C **82**, 035804 (2010).

[44] P. Raghavan, At. Data Nucl. Data Tables **42**, 189 (1989).

[45] Y. Xu, S. Goriely, A. Jorissen, G. L. Chen, and M. Arnould, Astron. Astrophys. **549**, A106 (2013).

[46] S. Goriely, E. Khan, and M. Samyn, Nucl. Phys. A **739**, 331 (2004).

[47] M. Martini, S. Peru, S. Hilaire, S. Goriely, and F. Lechaftois, Phys. Rev. C **94**, 014304 (2016).

[48] S. Goriely, S. Hilaire, S. Peru, and K. Sieja, Phys. Rev. C **98**, 014327 (2018).

[49] Y. Xu, S. Goriely, and E. Khan, Phys. Rev. C **104**, 044301 (2021).

[50] G. R. Satchler, *Direct Nuclear Reactions* (Clarendon Press, Oxford, 1983).

[51] H. Oberhummer, W. Balogh, R. Bieber, H. Herndl, U. Langer, T. Rauscher, and H. Beer, in *International Conference on Exotic Nuclei and Atomic Masses*, edited by M. de Saint Simon and O. Sorlin (Editions Frontières, Gif-sur-Yvette, France, 1995), p. 649.

[52] R. Capote *et al.*, Nucl. Data Sheets **110**, 3107 (2009).

[53] S. Goriely, S. Hilaire, and A. J. Koning, Phys. Rev. C **78**, 064307 (2008).

[54] P. M. Endt, At. Data Nucl. Data Tables **19**, 23 (1977).

[55] C. Iliadis and M. Wiescher, Phys. Rev. C **69**, 064305 (2004).

[56] K. Sieja and S. Goriely, Eur. Phys. J. A **57**, 110 (2021).

[57] N. K. Timofeyuk, P. Descouvemont, and R. C. Johnson, Eur. Phys. J. A **27**, 269 (2006).

[58] G. D'Agata *et al.*, Phys. Rev. C **103**, 015806 (2021).

[59] A. J. Koning and J. P. Delaroche, Nucl. Phys. A **713**, 231 (2003).

[60] E. Bauge, J. P. Delaroche, and M. Girod, Phys. Rev. C **63**, 024607 (2001).

[61] J. P. Jeukenne, A. Lejeune, and C. Mahaux, Phys. Rev. C **16**, 80 (1977).

[62] E. Bauge, J. P. Delaroche, M. Girod, G. Haouat, J. Lachkar, Y. Patin, J. Sigaud, and J. Chardine, Phys. Rev. C **61**, 034306 (2000).

[63] H. Scheit, F. Maréchal, T. Glassmacher, E. Bauge, Y. Blumenfeld, J. P. Delaroche, M. Girod, R. W. Ibbotson, K. W. Kemper, J. Libert, B. Pritychenko, and T. Suomijärvi, Phys. Rev. C **63**, 014604 (2000).

[64] E. Bauge, J. P. Delaroche, and M. Girod, Phys. Rev. C **58**, 1118 (1998).

[65] Y. Xu, S. Goriely, D. L. Balabanski, S. Chesnevskaya, G. L. Guardo, M. La Cognata, H. Y. Lan, D. Lattuada, W. Luo, and C. Matei, EPJ Web Conf. **178**, 04007 (2018).

[66] H. Y. Lan, Y. Xu, W. Luo, D. L. Balabanski, S. Goriely, M. La Cognata, C. Matei, A. Anzalone, S. Chesnevskaya, G. L. Guardo, D. Lattuada, R. G. Pizzone, S. Romano, C. Spitaleri, A. Taffara, A. Tumino, and Z. C. Zhu, Phys. Rev. C **98**, 054601 (2018).

[67] J. L. Zyskind *et al.*, Nucl. Phys. A **315**, 430 (1979).

[68] S. R. Kennett *et al.*, J. Phys. G **5**, 399 (1979).

[69] G. A. Krivonosov *et al.*, Izv. Rossiiskoi Akademii Nauk, Ser. Fiz. **41**, 2196 (1977).

[70] M. Rios, B. D. Anderson, and J. S. Schweitzer, Nucl. Phys. A **236**, 523 (1974).

[71] C. W. Cheng and J. D. King, Can. J. Phys. **58**, 1677 (1980).

[72] A. Simon *et al.*, Phys. Rev. C **87**, 055802 (2013).

[73] T. H. Hall *et al.*, Can. J. Phys. **53**, 445 (1975).

[74] C. I. W. Tingwell *et al.*, Nucl. Phys. A **439**, 371 (1985).

[75] S. Harissopulos, A. Spyrou, A. Lagoyannis, M. Axiotis, P. Demetriou, J. W. Hammer, R. Kunz, and H. W. Becker, Phys. Rev. C **87**, 025806 (2013).

[76] T. Sauter and F. Käppeler, Phys. Rev. C **55**, 3127 (1997).

[77] J. Hasper *et al.*, J. Phys.: Conf. Ser. **202**, 012005 (2010).

[78] N. Özkan *et al.*, Nucl. Phys. A **710**, 469 (2002).

[79] I. Dillmann *et al.*, Phys. Rev. C **84**, 015802 (2011).

[80] F. R. Chloupek, A.St J. Murphy, R. N. Boyd, A. L. Cole, J. Görres, R. T. Guray, G. Raimann, J. J. Zach, T. Rauscher, J. V. Schwarzenberg, P. Tischhauser, and M. C. Wiescher, Nucl. Phys. A **652**, 391 (1999).

[81] Gy. Gyürky *et al.*, Phys. Rev. C **95**, 035805 (2017).

[82] U. Hager *et al.*, Phys. Rev. C **85**, 035803 (2012).

[83] C. Rolfs, W. S. Rodne, M. H. Shapiro, and H. Winkler, Nucl. Phys. A **241**, 460 (1975).

[84] S. Harissopulos *et al.*, Eur. Phys. J. A **9**, 479 (2000).

[85] P. B. Lyons, J. W. Toevs, and D. G. Sargood, Nucl. Phys. A **130**, 1 (1969).

[86] T. Rauscher and F.-K. Thielemann, At. Data Nucl. Data Tables **75**, 1 (2000).

[87] R. H. Cyburt, A. M. Amthor, R. Ferguson, Z. Meisel, K. Smith, S. Warren, A. Heger, R. D. Hoffman, T. Rauscher, A. Sakharuk, H. Schatz, F.-K. Thielemann, and M. Wiescher, Astrophys. J. Suppl. Series **189**, 240 (2010).